PHOTONICS Research

Towards an optimum saturable absorber for the multi-gigahertz harmonic mode locking of fiber lasers

Jakub Bogusławski,[1,2,*] Grzegorz Soboń,[2] Rafał Zybała,[3,4] and Jarosław Sotor[2]

[1]Department of Physical Chemistry of Biological Systems, Institute of Physical Chemistry, Polish Academy of Sciences, Kasprzaka 42/44, 01-224 Warsaw, Poland
[2]Laser & Fiber Electronics Group, Faculty of Electronics, Wrocław University of Science and Technology, Wybrzeże Wyspiańskiego 27, 50-370 Wrocław, Poland
[3]University Research Center Functional Materials, Warsaw University of Technology, Wołoska 141, 02-507 Warsaw, Poland
[4]Institute of Electronic Materials Technology, Wólczyńska 133, 01-919 Warsaw, Poland
*Corresponding author: jakub.boguslawski@pwr.edu.pl

Received 8 May 2019; revised 4 July 2019; accepted 25 July 2019; posted 25 July 2019 (Doc. ID 366135); published 28 August 2019

Ultra-high-pulse-repetition-rate lasers are essential for a number of applications, including, e.g., optical communication and ablation-cooled material processing. Despite several techniques to generate pulses with gigahertz-range repetition rate, incorporating mainly short-length resonators, more widespread applications are still limited by the lack of a robust, simple, and cost-effective solution. Here, we report for the first time, to the best of our knowledge, fully passive harmonic mode locking in an all-polarization-maintaining (PM) fiber laser. The design guarantees a fixed polarization state and stable operation, where the cavity harmonic number is controlled by the pump power only. Self-starting operation is provided by the antimony telluride (Sb_2Te_3) thin-film saturable absorber (SA), which facilitates multiple pulse operation. The SA acts by means of low modulation depth, low saturation fluence, and an inverse slope in the saturable absorption curve. The optimum features of the SA and limiting factors for high-repetition-rate pulse generation in this regime of operation are discussed. As a result, 2.2 ps pulses with 3 GHz repetition rate are generated at 1560 nm wavelength. The study reports a new approach towards an optimal SA for multi-gigahertz pulse generation in practical, all-PM fiber lasers.

https://doi.org/10.1364/PRJ.7.001094

1. INTRODUCTION

Femtosecond lasers are currently an indispensable tool for precise material processing in scientific, industrial, and medical applications [1]. Recently, ablation-cooled material removal has been identified as a promising technique for reducing necessary pulse energy and increasing the efficiency of the removal process. In this regime, a pulse repetition rate has to be sufficiently high so that the ablated material will not cool down substantially before the arrival of the next pulse. Consequently, a pulse energy ablation threshold is reduced by several orders of magnitude, but the repetition rate has to reach GHz range [2]. Ultra-high-repetition-rate pulsed lasers are therefore highly desired for this application.

Fiber laser systems have shown great potential for this application [3–6]. Laser sources reported so far are typically realized in a chirped-pulse amplification (CPA) scheme [7] with a GHz-range oscillator being the heart of the system. There are a number of techniques to generate high-repetition-rate pulses in fiber oscillators. One approach is to construct a very short laser cavity [8,9], which is technically very challenging. Nonetheless, a repetition rate exceeding 19 GHz was achieved, but it required the cavity to be as short as 5 mm [9]. Another approach is to exploit passive harmonic mode locking in which multiple equidistant pulses are induced in the cavity, effectively increasing the repetition rate. A repetition rate reaching 22 GHz has been reported [10]. Most of those lasers are, however, mode locked using a nonlinear polarization evolution technique [10–12], which is extremely prone to external conditions and therefore not suitable for real-world applications. Targeting a specific harmonic number (and hence a desired repetition rate) requires careful adjustment of pump power and polarization state in the cavity. Moreover, this solution does not provide a fixed polarization state at the laser output. Those constraints could be addressed by designing a laser using polarization-maintaining (PM) fibers. This has been done in an early work by Roth *et al.*, where eighth harmonic (463 MHz) in an erbium-doped fiber laser was demonstrated, but additional optical pumping of a saturable Bragg reflector was required to obtain stable operation [13]. Harmonically mode-locked lasers operating with gigahertz repetition rate have been also

demonstrated using a variety of nanomaterial-based saturable absorbers (SAs), e.g., graphene [14], transition metal dichalcogenides (MoS_2 [15,16], WS_2 [17]), bismuth telluride [18,19], and black phosphorus [20]. Nevertheless, fully passive harmonic mode-locking operation has not yet been demonstrated in all-PM lasers, which would allow for environmentally stable, self-starting operation with a well-defined linearly polarized beam at the output.

This issue was solved in actively mode-locked fiber lasers. This technique allows for stable, turn-key operation and can be realized in all-PM fiber architecture [21]. Extremely high repetition rates exceeding 100 GHz were reported [8]. Despite those advantages, actively mode-locked fiber lasers are much more complex than passively modulated counterparts, as an amplitude (or phase) modulator and signal generator are required. An attempt to simplify the design of actively mode-locked lasers has been made by employing a compact graphene-based electro-optic modulator [22]. Nevertheless, repetition rates in GHz range have not been reported yet. This shows that an optimal solution for environmentally stable, simple, and cost-effective generation of ultra-high-repetition-rate pulses has not been proposed so far.

Here we report, for the first time, fully passive harmonic mode locking with ultra-high repetition rate in an all-PM fiber laser. The all-PM design allows for stable, self-starting operation with a fixed linear polarization state at the output. The harmonic mode-locking state is controlled by the pump power only. This feature is enabled by unique properties of the Sb_2Te_3 thin-film SA. Specifically, an inverse slope in saturable absorption observed for higher pulse energies induces multiple pulses in the laser cavity [23]. When the energy of the pulse increases, an induced loss increases as well; therefore, the pulse experiences higher losses. A multiple-pulse solution (each pulse with less energy) is favored, as it has less loss per round-trip than a single-pulse solution. On the other hand, the SA provides sufficiently low saturation fluence. Due to those features, pulses with maximum repetition rate of 3 GHz are generated. The harmonic number (corresponding to a specific repetition rate) is set by adjusting the pump power, and no further operations are needed. The laser works in a regime where repetition rate grows exponentially as a function of pump power, which allows for a more efficient use of the pump. The study is done in an erbium-doped fiber laser operating at 1560 nm with 2.2 ps pulses and 19.2 mW of average power at the highest harmonic number. We show that the available modulation depth of the SA limits the achievable repetition rate in this operation regime. The presented solution may be considered as a compact, simple, and robust seeding source for high-repetition-rate, high-power CPA systems for ablation-cooled material removal and other applications. The concept can be expanded for other wavelengths of operation, e.g., in 2 μm range in thulium- and holmium-doped fiber lasers.

2. SATURABLE ABSORBER PREPARATION AND CHARACTERIZATION

A thin-film Sb_2Te_3 SA is deposited directly on the tip of a PM fiber connector using a type of physical vapor deposition (PVD), namely, pulsed magnetron sputtering technique [24]. The method offers high-quality material deposition with a possibility to control its thickness [25].

First, antimony telluride compound is synthesized using tellurium powder and granules of antimony, both with purity >99.99%. To obtain a solid Sb_2Te_3, a mix of elementary powders in stoichiometric proportions is sealed in quartz ampules under vacuum (1 h at 950 K, followed by slow cooling down). Ampules are rocked throughout the process to ensure proper mixing of the alloy components. After cooling down, the obtained ingots are mechanically milled. Next, the attained powder is sintered using sink plasma sintering (SPS) technique [26]. The PVD itself is realized using a single planar magnetron (WMK-50) driven by a DORA Power System. The process is performed in a standard batch-type vacuum system in 0.25 Pa argon (Ar) atmosphere with current of 0.05 A and effective power of 0.03 kW. Further details regarding the fabrication process can be found in Ref. [24]. The fiber connector with angled physical contact (FC/APC) is mounted vertically on a rotating table (30 r/min) together with a microscopic glass slide for further characterization. The deposition time is set to 10 s. A scanning electron microscope (SEM) image of the sample deposited on a glass slide is presented in Fig. 1(a). The image shows a smooth and uniform surface. The SA is formed by connecting a Sb_2Te_3-deposited fiber connector with a clean one using a mating sleeve.

The nonlinear transmittance of the fabricated SA is measured using a fiber-based power-scan setup [27]. As a laser source, we use an Er-doped fiber laser with a pulse duration of 1 ps, repetition rate of 100 MHz, and central wavelength of 1560 nm. The measurement is performed using linearly polarized light. The obtained data [see Fig. 1(b)] are fitted

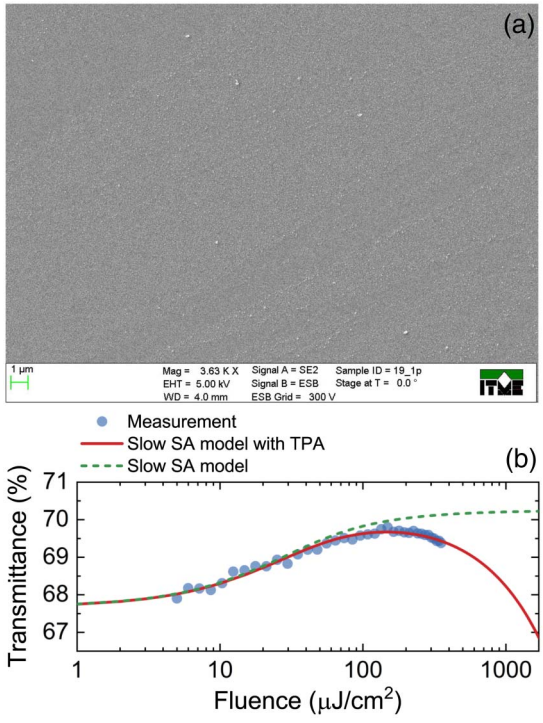

Fig. 1. Characterization of the SA. (a) SEM image of the surface of the Sb_2Te_3 layer. (b) Nonlinear transmittance of the Sb_2Te_2 SA fitted with a slow SA model with TPA. Dashed line shows a simulated nonlinear transmittance when the TPA is not included.

using a slow SA model describing the relationship between transmittance T and pulse fluence F_p [28]:

$$F_p = \alpha_{ns} - \left(1 - e^{\frac{-F_p}{F_{sat}}}\right) \cdot \frac{\Delta T \cdot F_{sat}}{F_p} - \frac{F_p}{F_2}, \quad (1)$$

from which resultant fitting parameters can be retrieved. We determine a modulation depth $\Delta T = 1.99\%$, nonsaturable losses $\alpha_{ns} = 29.75\%$, and a saturation fluence $F_{sat} = 16.4\ \mu J/cm^2$. An inverse slope in the saturable absorption curve is clearly visible and is described by the F_2 parameter, which indicates the fluence where the SA transmittance drops to 37% ($1/e$). Its origin is associated with a second-order nonlinear process, such as two-photon absorption (TPA), but other phenomena such as free-carrier absorption or thermal effects may also contribute [29]. Here, the F_2 parameter is also retrieved from Eq. (1) and is equal to 505 $\mu J/cm^2$, showing a fluence range where the roll-off effect becomes substantial. For comparison, with a dashed line, we show the calculated nonlinear transmittance using a slow SA model when no TPA is present.

3. DESIGN GUIDELINES AND EXPERIMENTAL SETUP

It has been pointed out that the presence of the inverse slope in a saturable absorption curve may be beneficial. It can be used to expand the stability range of mode-locking operation against Q-switching instabilities and to induce multiple-pulse operation at the same time [23,30]. The latter feature can be exploited for harmonic mode-locking operation. As energy of the pulses increases, a TPA-induced loss increases as well. In this case, a multiple-pulse solution will be favored, as it has less loss per round-trip than a single-pulse solution.

A pulse formation in fiber lasers is governed not only by the SA, but also by soliton pulse shaping [11]. The overall cavity design approach is to construct a soliton laser with excess energy, so that a high-energy pulse will break up and form multiple pulses, effectively increasing a repetition rate. In soliton area theorem, pulse energy E_p is limited by a fundamental soliton condition [31]:

$$E_p = \frac{2|\beta_{2,avg}|}{\tau \cdot \gamma_{avg}}, \quad (2)$$

where $\beta_{2,avg}$ is average cavity group velocity dispersion, γ_{avg} is average cavity nonlinearity, and τ is full width at half-maximum (FWHM) pulse duration divided by 1.7627. The equation shows that by decreasing the dispersion or increasing the nonlinearity, the average soliton energy can be lowered, thus facilitating a faster split up of the pulse as a function of pump power [32].

The experimental setup of the laser cavity is presented in Fig. 2. The entire laser is based on PM components and fibers in monolithic configuration, which guarantees immunity to external factors and stability of operation. The design is intended to be as simple as possible, hence comprising a filter-type hybrid component, which combines features of a wavelength-division multiplexer, an isolator, and a 30% output coupler. The SA is placed after the output coupler. The gain medium is 35 cm long erbium-doped fiber (Liekki Er80-4/125-PM, $\beta_2 = 58{,}000\ fs^2/cm$, $\gamma = 3.3\ W^{-1} \cdot km^{-1}$), which is pumped by a linearly polarized 980 nm laser diode in counter-propagating

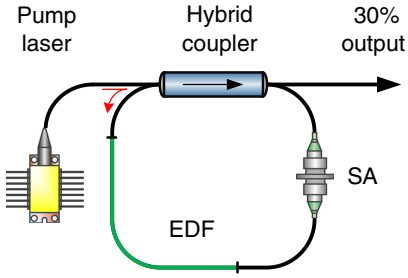

Fig. 2. Setup of ultra-simple all-PM fiber laser. EDF, erbium-doped fiber; SA, saturable absorber.

configuration. The remaining part of the cavity is composed of 223 cm long passive fiber (Nufern PM1550XP, $\beta_2 = -23{,}000\ fs^2/m$, $\gamma = 1.3\ W^{-1} \cdot km^{-1}$). The active fiber with normal dispersion is chosen to decrease the average cavity dispersion by compensating for anomalous dispersion of passive fibers. Furthermore, we choose the gain fiber with high nonlinearity, which helps to increase the average nonlinearity of the cavity. Consequently, considering the total cavity length of 258 cm, the average cavity dispersion and nonlinearity are $-0.1\ ps^2/m$ and $1.6\ W^{-1} \cdot km^{-1}$, respectively.

The laser operation is monitored using an optical spectrum analyzer (Yokogawa AQ6374), an optical autocorrelator (APE PulseCheck), a 6 GHz digital oscilloscope (Agilent Infiniium DSO91304A), and a 7 GHz radio frequency (RF) spectrum analyzer (Agilent EXA N9010A) connected to a fast photodiode (Discovery Semiconductors DSC2-50S) with 16 GHz bandwidth. The polarization state of the output beam is analyzed with a polarimeter (Thorlabs PAX7510IR1-T).

4. EXPERIMENTAL AND NUMERICAL RESULTS

A. Fundamental Mode Locking

The oscillator can be readily mode locked with fundamental repetition of 80.07 MHz with the broadest optical spectrum at the pump power of 37.5 mW. A detailed characterization of the laser operation at this pump power is shown in Fig. 3. The laser generates $sech^2$-shaped pulses, which is typical for cavities with net anomalous dispersion. Spectral width and central wavelength are 3.1 nm and 1560 nm, respectively. It is noteworthy that there are no Kelly sidebands visible in the spectrum [see Fig. 3(a)], which could potentially limit the obtainable pulse duration [33]. The lack of sidebands is also beneficial in terms of soliton amplification efficiency [34,35]. Figure 3(b) depicts the pulse autocorrelation together with hyperbolic secant fitting function, showing a 890 fs pulse duration. With a time-bandwidth product (TBP) of 0.34, the measurement results indicate that pulses are only slightly chirped. The RF spectrum of a pulse train features a broad spectrum of harmonics, confirming a stable mode-locking operation [Fig. 3(c)]. Signal-to-noise ratio (SNR) of the fundamental beat note is equal to 65 dB. The average output power is 1.2 mW, which translates to 15 pJ pulse energy (corresponding to intra-cavity pulse energy of 50 pJ).

We further analyze the laser operation by numerically simulating pulse propagation inside the cavity. The simulations are

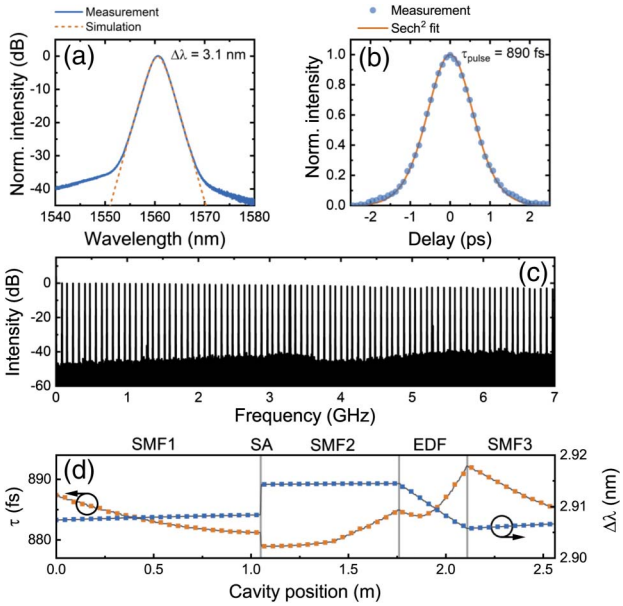

Fig. 3. Fundamental mode-locking operation. (a) Measured and simulated optical spectrum. (b) Autocorrelation trace of the output pulse with sech^2 fit. (c) RF spectrum in 7 GHz range. (d) Simulated pulse duration (τ) and spectral width ($\Delta\lambda$) evolution along the oscillator cavity; starting point is the output coupler.

performed by solving a generalized nonlinear Schrödinger equation by split-step Fourier method [36]. An initial pulse with 1 ps duration was seeded into a laser loop and its evolution was monitored over several hundreds of roundtrips until a steady state was reached. The simulation results shown in Fig. 3(d) indicate a moderate variation of pulse duration and spectral width along the oscillator cavity. This behavior is typical for soliton lasers operating with relatively low pulse energy (obtained in-cavity pulse energy of 53 pJ). The calculated optical spectrum exactly matches the experimental result with 2.9 nm width [Fig. 3(a)]. The predicted pulse duration is 890 fs after propagation in 1 m long out-coupling fiber.

B. Harmonic Mode Locking: Discussion

In harmonic mode locking, pulse characteristics depend on the pump power. Figure 4 summarizes laser parameters obtained in our experiment at different pumping powers and harmonic numbers. Figure 4(a) shows the dependence between the average output power and pump power, which was increased up to 19.2 mW for the highest harmonic number. A typical feature of a non-PM harmonically mode-locked laser is that it requires careful adjustment of polarization state while increasing pumping power to obtain a stable operation at a given harmonic frequency [37]. Here, due to the all-PM design, higher harmonic states are easily achieved simply by increasing the pump power. Figure 4(b) shows the measured repetition rates recorded at various pump powers. Unlike in typical harmonic mode-locked lasers [10], here this dependency is not linear, but nicely fitted with exponential function. The origin of this nonlinear characteristic is described in the next paragraphs. The maximum repetition rate reaches 3.04 GHz corresponding to 38th cavity harmonic, at relatively low pumping power of 320 mW. Stable pulse operation was not possible for higher pumping powers. To further analyze the laser behavior, for each harmonic number, we calculate a soliton order of the pulse propagating inside the cavity [31]. We take into account the average cavity nonlinearity and dispersion, as given in Section 3, as well as measured pulse duration. Given the small changes in soliton pulse during propagation, we assume that pulse duration inside the cavity is similar to the measured after the output coupler. The peak power has been approximated using measured average power (taking into account the output coupler splitting ratio), pulse duration, and the repetition rate. As shown in Fig. 4(c), for all harmonic numbers, the soliton order is maintained within 1.08–1.28 range. The laser adjusts the number of pulses in the cavity in order to fulfill a fundamental soliton criterion [31].

To further explore the behavior of the laser, we analyze the intra-cavity pulse fluence in the plane of the SA (i.e., working point) at various harmonic orders. Table 1 summarizes laser operation parameters obtained at various harmonic orders recorded during continuous increasing of pump power. Some of the points, 3rd, 7th, and 12th harmonics, were not included in this analysis, as they were recorded after slight decreasing of the pump power and may display different properties due to the hysteresis phenomenon [38]. Selected working points are plotted over the SA characteristic and shown in Fig. 5(a). As evident, the working point on the SA curve shifts towards lower fluence for increasing harmonic number and consequently the modulation depth "seen" by each pulse gradually decreases. As a result of lower effective modulation depth, the pulse duration is progressively increasing (from 890 fs to 2.2 ps) and spectral width is decreasing (from 3.1 to 1.8 nm), which is typical for mode-locking techniques [39]. The output pulse energy decreases from 15 pJ for fundamental mode locking to 6.3 pJ for 38th harmonic. Stable operation with such small pulse energies

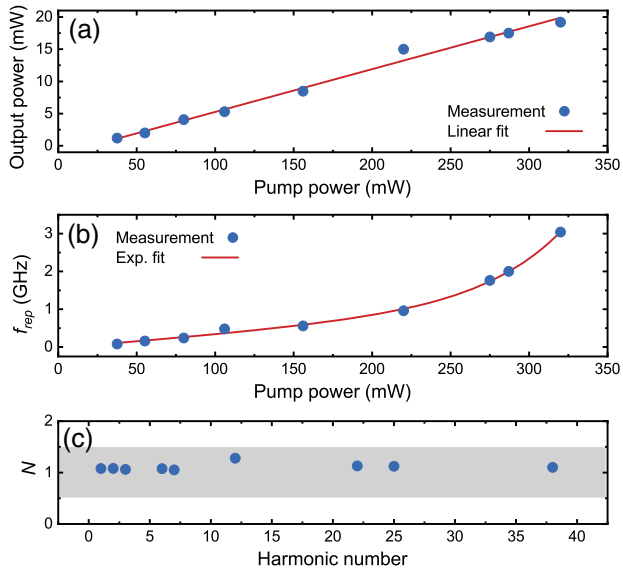

Fig. 4. Laser performance at various harmonic numbers. (a) Output power versus pump power with linear fit. (b) Repetition rate (f_{rep}) as a function of pump power with exponential fit. (c) Calculated soliton order (N) as a function of harmonic number; gray area indicates where fundamental soliton condition is fulfilled.

Table 1. Summary of the Achieved Laser Parameters Recorded during Continuous Increasing of Pump Power[a]

Harmonic Order	P_{out} (mW)	E_p (pJ)	f_{rep} (MHz)	$\Delta\lambda$ (nm)	τ (ps)	F_{WP} (μJ/cm^2)	ΔP_p (mW)
1	1.2	15.0	80.07	3.1	0.89	57.7	–
2	2.0	12.5	160.14	2.5	1.07	48.1	28.7
6	5.3	11.0	480.44	2.2	1.20	42.5	13.1
22	16.9	9.6	1761.61	1.9	1.54	36.9	9.8
25	17.5	8.7	2001.83	1.6	1.65	33.7	8.5
38	19.2	6.3	3042.75	1.8	2.20	24.3	5.2

[a]P_{out}, average output power; E_p, pulse energy; f_{rep}, repetition rate; $\Delta\lambda$, optical bandwidth (FWHM); τ, pulse duration; F_{WP}, intra-cavity pulse fluence at the SA (working point); ΔP_p, pump power stability range.

is enabled by the low saturation fluence of the SA, which is the key feature enabling high-repetition-rate operation.

Another consequence of decreased effective modulation depth is the progressively narrowing range of pumping power available for stable operation at each harmonic number (see Table 1). This range decreases from 28.7 mW for 2nd harmonic to 5.2 mW for the highest recorded harmonic. Consequently, smaller modulation depth translates into faster break-up into multiple pulses. A rate at which the modulation depth changes can be illustrated as the first derivative of the SA curve with respect to the pulse fluence ($\frac{dT}{dF}$). As depicted in Fig. 5(b), the derivative decreases exponentially, which means larger changes in modulation depth for lower fluences. This translates into nonlinear, exponential growth of the repetition rate as a function of pump power, as seen in Fig. 4(b). Multi-gigahertz repetition rates can be obtained much faster, at relatively small pumping powers. This way, the pump is used more efficiently, when compared to the regime where repetition rate grows linearly. At 38th harmonic, the effective modulation depth is ~1.2%. Stable operation for higher pumping powers is not possible, and further growth is limited by the available modulation depth of the SA, unlike in most cases where available pump power is the limiting factor [40]. This points to one potential constraint, where achievable repetition rate is ultimately limited by the available modulation depth of the SA, which also decreases pump power stability range. To obtain higher repetition rate, an SA with even lower saturation fluence and higher modulation depth would be beneficial.

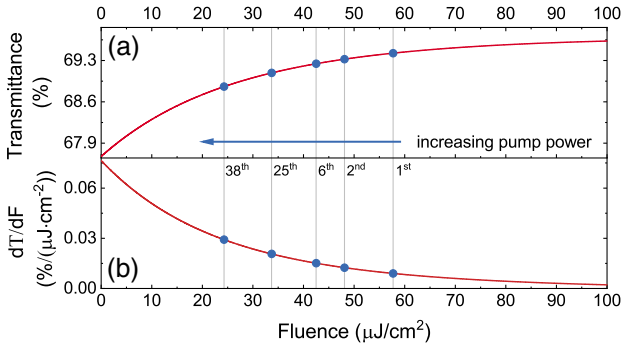

Fig. 5. Analysis of the working point of the SA. (a) Selected working points of the SA recorded during increasing the pump power plotted on the SA curve (*x* axis in linear scale). (b) First derivative of nonlinear transmittance curve with respect to fluence.

C. Harmonic Mode Locking: 3 GHz Operation

A detailed characterization of laser operation at 38th harmonic with maximum repetition rate of 3.04 GHz is presented in Fig. 6. The optical spectrum with 1.8 nm spectral width is characterized by a smooth shape and no Kelly sidebands are visible [Fig. 6(a)]. The autocorrelation trace shown in Fig. 6(b) gives 2.2 ps pulse duration. Calculated TBP is 0.49. The RF spectrum measured in 7 GHz span is presented in Fig. 6(c). Supermode noise peaks are RF beat notes at integer multiplies of the fundamental cavity frequency, and their suppression is one of the basic measures of harmonic mode-locking quality [41]. We estimate supermode suppression according to the definition given in Ref. [42], as an SNR between carrier frequency and the average power level of the supermode noise peaks. The obtained value of 40 dB is higher than the previously reported for a laser operating with similar repetition rate [37]. Figure 6(d) shows the 3.04 GHz RF beat note measured in 500 kHz span. The recorded oscilloscope trace of equally spaced output pulses is characterized by good amplitude stability [<7%, Fig. 6(e)]. The average output power is 19.2 mW, corresponding to the single pulse energy of 6.3 pJ. Furthermore, due to the all-PM configuration the performance is reproducible after each start-up of the laser. It is possible to preset the pump power, and the laser immediately starts to operate at a given harmonic number after starting the pump power.

Finally, the polarization state of the output beam is analyzed to confirm if it is linear. Figure 7 shows the degree of polarization (DOP) versus azimuth of polarization of 1024 samples measured over the period of 60 s. Both DOP and polarization azimuth are also presented in the form of histograms.

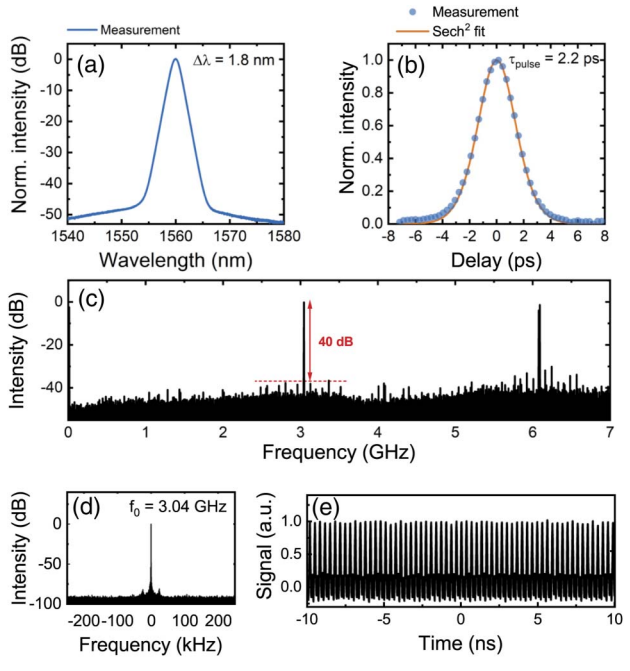

Fig. 6. Harmonic mode-locking operation of 38th order. (a) Optical spectrum. (b) Autocorrelation trace of the output pulse with sech^2 fit. (c) RF spectrum in 7 GHz range. (d) 3.04 GHz beat note of RF spectrum measured in 500 kHz span. (e) Oscilloscope trace of output pulses.

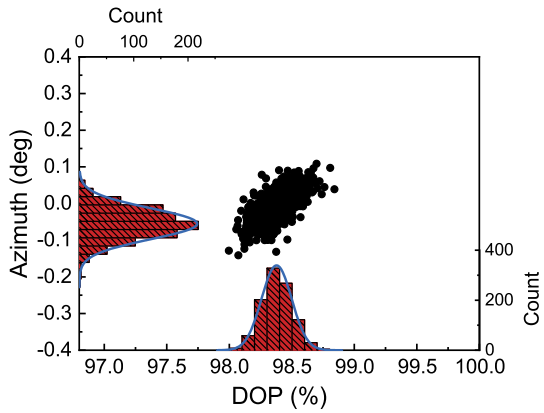

Fig. 7. Polarization properties of output beam. Polarization azimuth versus degree of polarization (DOP) with measured period of 60 s.

The DOP has a mean value of 98.4% with standard deviation of 0.12%. The mean value of azimuth is −0.006° with standard deviation of 0.04°. These values are comparable to previously reported all-PM lasers [43]. Consequently, the laser produces a linearly polarized beam with very good stability.

5. CONCLUSION

In conclusion, we have reported fully passive harmonic mode locking in an all-PM Er-doped fiber laser. In this architecture, stable multi-gigahertz harmonic operation was enabled by the Sb_2Te_3 thin-film SA. We have studied the mode of laser operation where repetition rate grows exponentially as a function of pump power. This enables 3 GHz repetition rate operation at relatively low pumping power. We have identified key features of the SA, which are beneficial for multi-gigahertz operation, namely, low saturation fluence and the inverse slope in the SA curve, which prevents a single-pulse solution. With a combination of those properties, 2.2 ps pulses were generated with 3 GHz repetition rate and 19.2 mW output power. We have also discussed potential limitations of this mode of operation, where achievable repetition rate is ultimately limited by the available modulation depth of the SA. Due to the all-PM architecture, the laser can be simply mode locked by setting the pump power above the threshold, and the specific repetition rate can be reached by further increasing the power. The laser produces a fixed, linear polarization at the output. This further confirms that Sb_2Te_3 can be a promising material for the application as an SA for multi-gigahertz operation of fiber lasers.

Funding. Narodowe Centrum Nauki (2014/13/N/ST7/01968, 2016/23/D/ST8/02686); Politechnika Wrocławska (0401/0030/18); Fundacja na rzecz Nauki Polskiej (FNP) (POIR.04.04.00-00-3D47/16-00).

Acknowledgment. We acknowledge the valuable help of Dr. Krzysztof Mars during the PVD deposition.

REFERENCES

1. S. H. Chung and E. Mazur, "Surgical applications of femtosecond lasers," J. Biophoton. **2**, 557–572 (2009).
2. C. Kerse, H. Kalaycoğlu, P. Elahi, B. Çetin, D. K. Kesim, Ö. Akçaalan, S. Yavaş, M. D. Aşk, B. Öktem, H. Hoogland, R. Holzwarth, and F. Ö. Ilday, "Ablation-cooled material removal with ultrafast bursts of pulses," Nature **537**, 84–88 (2016).
3. P. Elahi, Ö. Akçaalan, C. Ertek, K. Eken, F. Ö. Ilday, and H. Kalaycoğlu, "High-power Yb-based all-fiber laser delivering 300 fs pulses for high-speed ablation-cooled material removal," Opt. Lett. **43**, 535–538 (2018).
4. H. Kalaycoğlu, P. Elahi, Ö. Akçaalan, and F. Ö. Ilday, "High-repetition-rate ultrafast fiber lasers for material processing," IEEE J. Sel. Top. Quantum Electron. **24**, 8800312 (2018).
5. C. Kerse, H. Kalaycoğlu, P. Elahi, Ö. Akçaalan, and F. Ö. Ilday, "3.5-GHz intra-burst repetition rate ultrafast Yb-doped fiber laser," Opt. Commun. **366**, 404–409 (2016).
6. P. Elahi, H. Kalaycioğlu, Ö. Akçaalan, Ç. Şenel, and F. Ö. Ilday, "Burst-mode thulium all-fiber laser delivering femtosecond pulses at a 1 GHz intra-burst repetition rate," Opt. Lett. **42**, 3808–3811 (2017).
7. D. Strickland and G. Mourou, "Compression of amplified chirped optical pulses," Opt. Commun. **55**, 447–449 (1985).
8. H. Cheng, W. Wang, Y. Zhou, T. Qiao, W. Lin, Y. Guo, S. Xu, and Z. Yang, "High-repetition-rate ultrafast fiber lasers," Opt. Express **26**, 16411–16421 (2018).
9. A. Martinez and S. Yamashita, "Multi-gigahertz repetition rate passively modelocked fiber lasers using carbon nanotubes," Opt. Express **19**, 6155–6163 (2011).
10. S. Tao, L. Xu, G. Chen, C. Gu, and H. Song, "Ultra-high repetition rate harmonic mode-locking generated in a dispersion and nonlinearity managed fiber laser," J. Lightwave Technol. **34**, 2354–2357 (2016).
11. D. Tang, L.-M. Zhao, B. Zhao, and A. Liu, "Mechanism of multisoliton formation and soliton energy quantization in passively mode-locked fiber lasers," Phys. Rev. A **72**, 043816 (2005).
12. G. Semaan, A. Komarov, M. Salhi, and F. Sanchez, "Study of a harmonic mode lock stability under external continuous-wave injection," Opt. Commun. **387**, 65–69 (2017).
13. J. Roth, N. Bonadeo, K. Bergman, and W. Knox, "Polarisation-maintaining, harmonically modelocked soliton fibre laser with repetition rate stabilisation using optical pumping of saturable Bragg reflector," Electron. Lett. **38**, 16–17 (2002).
14. G. Sobon, J. Sotor, and K. M. Abramski, "Passive harmonic mode-locking in Er-doped fiber laser based on graphene saturable absorber with repetition rates scalable to 2.22 GHz," Appl. Phys. Lett. **100**, 161109 (2012).
15. M. Liu, X.-W. Zheng, Y.-L. Qi, H. Liu, A.-P. Luo, Z.-C. Luo, W.-C. Xu, C.-J. Zhao, and H. Zhang, "Microfiber-based few-layer MoS_2 saturable absorber for 2.5 GHz passively harmonic mode-locked fiber laser," Opt. Express **22**, 22841–22846 (2014).
16. Y. Wang, D. Mao, X. Gan, L. Han, C. Ma, T. Xi, Y. Zhang, W. Shang, S. Hua, and J. Zhao, "Harmonic mode locking of bound-state solitons fiber laser based on MoS_2 saturable absorber," Opt. Express **23**, 205–210 (2015).
17. J. Lee, J. Park, J. Koo, Y. M. Jhon, and J. H. Lee, "Harmonically mode-locked femtosecond fiber laser using non-uniform, WS_2-particle deposited side-polished fiber," J. Opt. **18**, 035502 (2016).
18. Z.-C. Luo, M. Liu, H. Liu, X.-W. Zheng, A.-P. Luo, C.-J. Zhao, H. Zhang, S.-C. Wen, and W.-C. Xu, "2 GHz passively harmonic mode-locked fiber laser by a microfiber-based topological insulator saturable absorber," Opt. Lett. **38**, 5212–5215 (2013).
19. J. Lee, J. Koo, Y. M. Jhon, and J. H. Lee, "Femtosecond harmonic mode-locking of a fiber laser based on a bulk-structured $BiTe_3$ topological insulator," Opt. Express **23**, 6359–6369 (2015).
20. M. Pawliszewska, Y. Ge, Z. Li, H. Zhang, and J. Sotor, "Fundamental and harmonic mode-locking at 2.1 μm with black phosphorus saturable absorber," Opt. Express **25**, 16916–16921 (2017).
21. M. Nakazawa and E. Yoshida, "A 40-GHz 850-fs regeneratively fm mode-locked polarization-maintaining erbium fiber ring laser," IEEE Photon. Technol. Lett. **12**, 1613–1615 (2000).
22. J. Bogusławski, Y. Wang, H. Xue, X. Yang, D. Mao, X. Gan, Z. Ren, J. Zhao, Q. Dai, G. Soboń, J. Sotor, and Z. Sun, "Graphene actively mode-locked lasers," Adv. Funct. Mater. **28**, 1801539 (2018).

23. E. Thoen, E. Koontz, M. Joschko, P. Langlois, T. Schibli, F. Kärtner, E. Ippen, and L. Kolodziejski, "Two-photon absorption in semiconductor saturable absorber mirrors," Appl. Phys. Lett. **74**, 3927–3929 (1999).
24. R. Zybała, K. Mars, A. Mikuła, J. Bogusławski, G. Soboń, J. Sotor, M. Schmidt, K. Kaszyca, M. Chmielewski, L. Ciupiński, and K. Pietrzak, "Synthesis and characterization of antimony telluride for thermoelectric and optoelectronic applications," Arch. Metal. Mater. **62**, 1067–1070 (2017).
25. P. Loiko, J. Bogusławski, J. M. Serres, E. Kifle, M. Kowalczyk, X. Mateos, J. Sotor, R. Zybała, K. Mars, A. Mikuła, K. Kaszyca, M. Aguiló, F. Díaz, U. Griebner, and V. Petrov, "Sb_2Te_3 thin film for the passive *Q*-switching of a Tm:$GDVO_4$ laser," Opt. Mater. Express **8**, 1723–1732 (2018).
26. R. Zybala and K. T. Wojciechowski, "Anisotropy analysis of thermoelectric properties of $Bi_2Te_{2.9}Se_{0.1}$ prepared by SPS method," AIP Conf. Proc. **1449**, 393–396 (2012).
27. G. Sobon, "Mode-locking of fiber lasers using novel two-dimensional nanomaterials: graphene and topological insulators," Photon. Res. **3**, A56–A63 (2015).
28. R. Grange, M. Haiml, R. Paschotta, G. Spühler, L. Krainer, M. Golling, O. Ostinelli, and U. Keller, "New regime of inverse saturable absorption for self-stabilizing passively mode-locked lasers," Appl. Phys. B **80**, 151–158 (2005).
29. M. Haiml, R. Grange, and U. Keller, "Optical characterization of semiconductor saturable absorbers," Appl. Phys. B **79**, 331–339 (2004).
30. T. Schibli, E. Thoen, F. Kärtner, and E. Ippen, "Suppression of *Q*-switched mode locking and break-up into multiple pulses by inverse saturable absorption," Appl. Phys. B **70**, S41–S49 (2000).
31. G. P. Agrawal, "Nonlinear fiber optics," in *Nonlinear Science at the Dawn of the 21st Century* (Springer, 2000), pp. 195–211.
32. C. S. Jun, S. Y. Choi, F. Rotermund, B. Y. Kim, and D.-I. Yeom, "Toward higher-order passive harmonic mode-locking of a soliton fiber laser," Opt. Lett. **37**, 1862–1864 (2012).
33. L. Nelson, D. Jones, K. Tamura, H. Haus, and E. Ippen, "Ultrashort-pulse fiber ring lasers," Appl. Phys. B **65**, 277–294 (1997).
34. J. Li, Y. Wang, H. Luo, Y. Liu, Z. Yan, Z. Sun, and L. Zhang, "Kelly sideband suppression and wavelength tuning of a conventional soliton in a Tm-doped hybrid mode-locked fiber laser with an all-fiber lyot filter," Photon. Res. **7**, 103–109 (2019).
35. C. W. Rudy, K. E. Urbanek, M. J. Digonnet, and R. L. Byer, "Amplified 2-μm thulium-doped all-fiber mode-locked figure-eight laser," J. Lightwave Technol. **31**, 1809–1812 (2013).
36. B. Oktem, C. Ülgüdür, and F. Ö. Ilday, "Soliton-similariton fibre laser," Nat. Photonics **4**, 307–311 (2010).
37. F. Amrani, A. Haboucha, M. Salhi, H. Leblond, A. Komarov, P. Grelu, and F. Sanchez, "Passively mode-locked erbium-doped double-clad fiber laser operating at the 322nd harmonic," Opt. Lett. **34**, 2120–2122 (2009).
38. A. Komarov, H. Leblond, and F. Sanchez, "Multistability and hysteresis phenomena in passively mode-locked fiber lasers," Phys. Rev. A **71**, 053809 (2005).
39. I. Jung, F. Kärtner, N. Matuschek, D. Sutter, F. Morier-Genoud, Z. Shi, V. Scheuer, M. Tilsch, T. Tschudi, and U. Keller, "Semiconductor saturable absorber mirrors supporting sub-10-fs pulses," Appl. Phys. B **65**, 137–150 (1997).
40. C. S. Jun, J. H. Im, S. H. Yoo, S. Y. Choi, F. Rotermund, D.-I. Yeom, and B. Y. Kim, "Low noise GHz passive harmonic mode-locking of soliton fiber laser using evanescent wave interaction with carbon nanotubes," Opt. Express **19**, 19775–19780 (2011).
41. F. Rana, H. L. Lee, R. J. Ram, M. E. Grein, L. A. Jiang, E. P. Ippen, and H. A. Haus, "Characterization of the noise and correlations in harmonically mode-locked lasers," J. Opt. Soc. Am. B **19**, 2609–2621 (2002).
42. O. Pottiez, O. Deparis, R. Kiyan, M. Haelterman, P. Emplit, P. Mégret, and M. Blondel, "Supermode noise of harmonically mode-locked erbium fiber lasers with composite cavity," IEEE J. Quantum Electron. **38**, 252–259 (2002).
43. S. Ko, J. Lee, J. Koo, and J. H. Lee, "Experimental investigation into generation of bursts of linearly-polarized, dissipative soliton pulses from a figure-eight fiber laser at 1.03 μm," Jpn. J. Appl. Phys. **57**, 032701 (2018).